South East Asian J. of Mathematics and Mathematical Sciences Vol. 19, No. 3 (2023), pp. 421-436

ISSN (Print): 0972-7752

# THERMAL DIFFUSION AND RADIATION ABSORPTION IMPACTS ON CHEMICALLY REACTIVE AND RADIATIVE NANOFLUID FLOW PAST AN EXPONENTIALLY ACCELERATED VERTICAL POROUS PLATE

# M. Santha Raju and G. S. S. Raju\*

Department of Mathematics, Dr. S. R. K. Government Arts College, Yanam - 533464, Andhra Pradesh, INDIA

E-mail: santharajusrkgac@gmail.com

\*Department of Mathematics, JNTUA College of Engineering, Pulivendula, Andhra Pradesh, INDIA

(Received: Feb. 19, 2022 Accepted: Nov. 20, 2023 Published: Dec. 30, 2023)

Abstract: The role of thermal diffusion (Soret) and radiation-absorption influences on the unsteady MHD boundary layer flow for Silver (Ag) and Copper (Cu) water-based nanofluid over an accelerated exponentially vertical porous plate has been investigated. The varying temperature and concentration at the plate are also considered. The governing equations of the flow are numerically resolved to employ the finite-difference system of the implicit Crank-Nicolson method. Fluid velocity, fluid temperature, and species concentration were all plotted for meaningful physical parameters. For both nanofluids, non-dimensional metrics such as the friction factor, Nusselt number, and Sherwood number at the surface are tabulated. The data obtained from the literature provide strong validation for the findings. The finding of the study is that both nanofluids' velocities rise with increases in Soret and radiation absorption parameters. For increased values of Soret and radiation absorption parameters, the friction factor and Nusselt number increase. Sherwood numbers drop for the Soret parameter and rise for the radiation absorption.

**Keywords and Phrases:** MHD, Nanofluid, radiation absorption, variable concentration, variable temperature, finite difference scheme.

**2020** Mathematics Subject Classification: 35Q35, 76M20, 76S05, 76W05, 80A32, 76M55.

# Nomenclature

TAGILLE	nciature		
a	Acceleration parameter	Sc	Schmidt number
$a', u_0$	Constants	So	Soret number
$B_0$	Applied magnetic field, $NmA^{-1}$	T	Dimensionless temperature
C	Fluid concentration	t	Time parameter
$C_P$	Specific heat at constant pressure, $Jkg^{-1}K$	T'	Temperature, K
C'	Species concentration, $Kgm^{-3}$	t'	Time, s
D	Mass-diffusion coefficient	U	Dimensionless velocity
$D_1$	Thermal diffusion coefficient	u	Velocity of the fluid along x-direction
g	Acceleration due to gravity, $ms^{-2}$	y	Spatial variable, m
Gr	Thermal Grashof number	Y	Dimensionless Spatial variable
Gc	Solutal Grashof number		Greek symbols
$K^*$	Permeability parameter	$\beta^*$	Mass transfer coefficient, $K^{-1}$
k	Thermal conductivity, $Wm^{-1}K^{-1}$	$\beta$	Thermal expansion coefficient, $K^{-1}$
K	Permeability of the porous medium, $m^2$	$\phi$	Nanoparticle volume fraction
$K_r^1$	Chemical reaction parameter	$\mu$	Dynamic viscosity, $m^2s^{-1}$
Kr	Dimensionless chemical reaction parameter	$\rho$	Density, $kgm^{-3}$
$k_e$	Mean-absorption coefficient, $m^{-1}$	$\sigma_s$	Stefan-Boltzman constant, $Wm^{-2}K^{-4}$
M	Magnetic parameter	$\sigma$	Electric conductivity, $m^2 s^{-1}$
Nu	Nusselt Number	au	Skin friction
Nr	Radiation parameter		Subscripts
Pr	Prandtl number	$\infty$	quantities at free stream
$Q_1$	Radiation absorption coefficient	f	base fluid
$Q_L$	Radiation absorption parameter	$\mathbf{s}$	nanoparticle
$q_r$	Radiative heat flux, $Wm^{-2}$	w	quantities at wall
Sh	Sherwood number	$_{ m nf}$	Nanofluid
_			

## 1. Introduction

Nanofluids are fluids that have improved thermal properties and are commonly used to enrich the effectiveness of heat transfer. Adding nanoparticles to a liquid can enhance its thermal properties and facilitate heat transmission which has been introduced by Choi [3]. While increasing heat transfer is desirable in many engineering applications, the magnetic field decreases the convective flux field. Magnetic field effects have enticed the attention of scientists and engineers owing to their vast range of industrial uses, including magnetohydrodynamic (MHD) generators, pumps, and bearings. Until the recent emergence of maritime applications in the processing of petroleum and natural gas, the flow of nanofluids in oscillating porous media has seldom been extensively investigated. Vertical oscillating plates are now used as heat exchangers in refrigerating systems, and there is increasing

interest in this type of flow in the offshore fossil fuel extraction and processing sector. Satya Narayana et al. [16, 17] analyzed MHD nanofluid flow, heat, and mass transfer past on a vertical plate in a rotating system. Mahanthesh et al. [6] investigated heat and mass transfer influence on MHD nanofluid flow past a stationary/moving plate. Rajesh et al. [9, 10] conferred MHD nanofluid flow across a vertical plate with variable surface temperature. Some motivating and inspiring work about MHD flow can be constituted in [2, 11, 15, 22].

The influence of density inequalities in the flow regime is substantial. When organisms are introduced at a surface in a fluid domain that has a different (lower) density than the surrounding liquid, thermal-diffusion (Soret) effects can be rather severe. Furthermore, the linkages between fluxes and driving abilities get more complex when heat mass transfer takes place simultaneously in a moving fluid. Sheikholeslami et al. [19] deliberate the influence of Soret and heat generation on the flow of MHD nanofluids through an oscillating porous plate. Reddy et al. [12-14] examined the influences of Soret and radiation on magneto-nanofluid flow through a moving vertical porous plate. Singha et al. [20] explored the thermal-diffusion and Diffusion-thermo impacts on the MHD flow of water-based nanofluids via exponentially expanding porous material sheet with variable surface concentration and temperature. Singh et al. [21] studied the thermal diffusion effect on MHD convective nanofluid flow via heated and magnetized surface with an induced magnetic field (IMF), magneto, and Hall current effects.

Another important component of fluid flow is the generation and absorption of heat. Applications in mechanical engineering, thermal engineering, physics, and the food industry can be made for procedures such as heat treatment, ventilation, and air conditioning. Satya Narayana [18] discussed the effects of radiation absorption and variable permeability on MHD nanofluid flow in the wavy channel. Venkateswarlu et al. [23] studied the influences of radiation absorption and chemical reaction on the flow of MHD nanofluids beyond a vertical plate in a rotational system. Prasad et al. [8] discussed the impact of radiation absorption on MHD convective nanofluid flow over a flat plate with Diffusion thermo and chemical reaction effects. Ameer Ahamad et al. [1] studied the impacts of radiation absorption and Dufour on MHD nanofluid flow on a vertically moving plate with a constant heat source. Krishna et al. [5] analyzed the influence of Radiation absorption on MHD nanofluid flow via a vertical porous plate with a transverse magnetic field.

The researchers mentioned above laid the foundation for this research. Upon conducting a thorough assessment of the literature, we found that no research has been done to date that looks at the effects of radiation absorption and Soret simultaneously with MHD convective nanofluid flow over an accelerated porous plate.

The work is unique in that it takes into account the impact of Soret and radiation absorption on the MHD radiating convective nanofluid flow through an accelerated exponentially porous plate with varying temperature and concentration. Water is a basic fluid that includes two kinds of nanoparticles: Copper (Cu) and Silver (Ag). The finite-difference approach of the Crank-Nicolson method is applied to resolve the resultant equations. The nondimensional characteristics of fluid velocity, fluid temperature, species concentration, Nusselt number, Sherwood number, and friction factor of the nanofluid were investigated using plots and tables.

# 2. Mathematical formulation

Consider the influence of Soret and the radiation absorption of a free convective flow of unstable MHD radiating nanofluid through an infinite vertical porous plate moving an exponentially accelerated movement. The influence of chemical reactions is also considered. The plate is initially at rest, with a temperature of  $T'_{\infty}$  and species concentration of  $C'_{\infty}$ . The plate accelerates exponentially with a velocity  $u = u_0 \exp(a't')$  in its plane, the temperature is maintained as  $T' = T'_{\infty} + A(T'_w - T'_{\infty})t'$ , and species concentration is maintained as  $C' = C'_{\infty} + A(C'_w - C'_{\infty})t'$  at time t' > 0. The x-axis is aligned vertically with the plate, whereas the y-axis is at the right angle to the plate as shown in Fig. 1. The flow is confined in the normal direction to the plate.

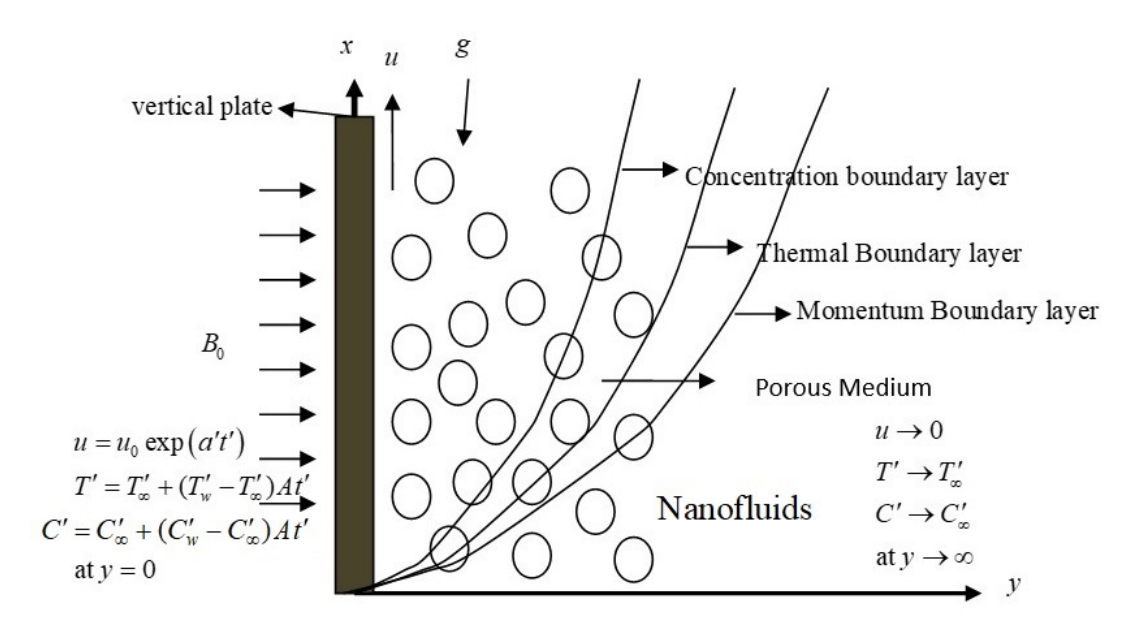


Figure 1: Physical diagram of the flow model

In this analysis the following assumptions are made:

- When a homogeneous magnetic field B of force  $B_0$  is applied in a normal direction to the plate and the fluid is supposed to be electrically conductive.
- Because the magnetic Reynolds number is small enough to overlook the effects of the induced magnetic field, the induced magnetic field created by fluid motion is minimal in comparison to the applied magnetic field. Since Reynolds' magnetic number is so low, this assumption is justified.
- In the normal direction, radiative heat flux is acted on to the plate.
- Fluid is a nano-fluid containing nanoparticles of copper or silver, similar to a water-based fluid. Table 1 lists the thermophysical parameters of the nanofluids.
- Thermal equilibrium is assumed for the water-base fluid and suspended nanoparticles.
- Consider density in the equation of mass being linearly proportional to temperature buoyancy forces.
- Because the polarization effects are expected to be negligible, the electric field is likewise supposed to be negligible.

Under the aforementioned assumptions, the momentum, energy, and species concentration equations with radiation absorption, and thermal diffusion past an exponentially accelerating plate can be stated as (Reddy et al. [14] and Krishna et al. [5]).

$$\frac{\partial u}{\partial t'} = \frac{\mu_{nf}}{\rho_{nf}} \frac{\partial^2 u}{\partial y^2} - \frac{\sigma_{nf} B_0^2 u}{\rho_{nf}} - \frac{\mu_{nf} u}{K \rho_{nf}} + \frac{(\rho \beta^*)_{nf}}{\rho_{nf}} g(C' - C_{\infty}') + \frac{(\rho \beta)_{nf}}{\rho_{nf}} g(T' - T_{\infty}')$$
(1)

$$\frac{\partial T'}{\partial t'} = \frac{k_{nf}}{(\rho C_P)_{nf}} \frac{\partial^2 T'}{\partial y^2} - \frac{1}{(\rho C_P)_{nf}} \frac{\partial q_r}{\partial y} + \frac{Q_1}{(\rho C_P)_{nf}} (C' - C'_{\infty}) \tag{2}$$

$$\frac{\partial C'}{\partial t'} = D \frac{\partial^2 C'}{\partial u^2} + D_1 \frac{\partial^2 T'}{\partial u^2} - K_r^1 (C' - C_\infty')$$
(3)

Corresponding the initial & boundary conditions are

$$u(y,0) = 0, T'(y,0) = T'_{\infty}, C'(y,0) = C'_{\infty} \quad \forall \quad y$$

$$u(0,t') = u_0 \exp(a't'), T'(0,t') = T'_{\infty} + A(T'_w - T'_{\infty})t',$$

$$C'(0,t') = C'_{\infty} + A(C'_w - C'_{\infty})t' \quad \forall \quad t' > 0$$

$$u(y,t') \to 0, T'(y,t') \to T'_{\infty}, C'(y,t') \to C'_{\infty} \quad \text{as } y \to \infty, t' > 0$$

$$(4)$$

where  $A = (u_0^2/v_f)$ .

Table 1. Thermo-physical properties of water, silver, and copper (Anwar et al. [2]; Mishra et al. [7]).

Physical properties	Water $(H_2O)$	Silver (Ag)	Copper (Cu)
k (W/mK)	0.613	429	401
$C_p (J/Kg K)$	4179	235	385
$\sigma (sm^{-1})$	$5.5 \times 10^{-6}$	$6.3 \times 10^{7}$	$59.6 \times 10^{6}$
$\beta \times 10^5 \ (K^{-1})$	21	1.89	1.67
$\rho (Kg/m^3)$	997.1	10500	8933

The expressions of  $(\rho C_P)_{nf}$ ,  $\sigma_{nf}$ ,  $(\rho\beta)_{nf}$ ,  $(\rho\beta^*)_{nf}$ ,  $\rho_{nf}$ ,  $\mu_{nf}$  are respectively given by

$$(\rho C_P)_{nf} = (1 - \phi)(\rho C_P)_f + \phi(\rho C_P)_s, \sigma_{nf} = \left[1 + \frac{3(\sigma - 1)\phi}{(\sigma + 2) - (\sigma - 1)\phi}\right]\sigma_f,$$

$$\sigma = \frac{\sigma_s}{\sigma_f}, (\rho\beta)_{nf} = (1 - \phi)(\rho\beta)_f + \phi(\rho\beta)_s, (\rho\beta^*)_{nf} = (1 - \phi)(\rho\beta^*)_f + \phi(\rho\beta^*)_s,$$

$$\rho_{nf} = \phi\rho_s + (1 - \phi)\rho_f, \mu_{nf} = \mu_f \frac{1}{(1 - \phi)^{2.5}}.$$
(5)

Hamilton and Crosser [4] model is used to deal with the thermal conductivity of nanofluids is given by

$$k_{nf} = \left[ \frac{k_s - 2(k_f - k_s)\phi + 2k_f}{\phi(k_f - k_s) + 2k_f + k_s} \right] k_f \tag{6}$$

We use the Rosseland approximation to model unidirectional radiative heat flux, which gives us the following radiative heat flux expression.

$$q_r = -\frac{4\sigma_s}{3k_e} \left[ \frac{\partial T^{\prime 4}}{\partial y} \right] \tag{7}$$

Using neglecting the higher-order parts in the expansion owing to small temperature fluctuations  $q_r$  is linearized by Taylor series expansion for  $T'^4$  around  $T'_{\infty}$ , which is given

$$T^{\prime 4} = 4[T^{\prime}T_{\infty}^{\prime 3}] - 3[T_{\infty}^{\prime 4}] \tag{8}$$

By applying Equations (7) and (8), Equation (2) results into

$$\frac{\partial T'}{\partial t'} = \frac{k_{nf}}{(\rho C_P)_{nf}} \frac{\partial^2 T'}{\partial y^2} + \frac{16\sigma_s T_{\infty}^{\prime 3}}{3k_e(\rho C_P)_{nf}} \frac{\partial^2 T'}{\partial y^2} + \frac{Q_1}{(\rho C_P)_{nf}} (C' - C_{\infty}') \tag{9}$$

Define

$$U = \frac{u}{u_0}, t = \frac{t'u_0^2}{v_f}, Y = \frac{yu_0}{v_f}, C = \frac{C' - C'_{\infty}}{C'_{w} - C'_{\infty}}, T = \frac{T' - T'_{\infty}}{T'_{w} - T'_{\infty}}, a = \frac{a'v_f}{u_0^2}$$
(10)

By using Eq. (10), Equations (1), (3), and (9) reduces

$$\frac{\partial U}{\partial t} = a_1 \frac{\partial^2 U}{\partial Y^2} - M^2 a_4 U - \frac{a_1}{K^*} U + Gr a_2 T + Gc a_3 C \tag{11}$$

$$\frac{\partial T}{\partial t} = \frac{1}{x_5 P r} \left( (x_6 + N r) \frac{\partial^2 T}{\partial Y^2} + Q_L C \right) \tag{12}$$

$$\frac{\partial C}{\partial t} = \frac{1}{Sc} \frac{\partial^2 C}{\partial Y^2} + So \frac{\partial^2 T}{\partial Y^2} - KrC \tag{13}$$

where

$$\begin{split} x_1 &= \left(1 - \phi + \phi \frac{\rho_s}{\rho_f}\right), x_2 = \left(1 - \phi + \phi \frac{(\rho\beta)_s}{(\rho\beta)_f}\right), x_3 = \left(1 - \phi + \phi \frac{(\rho\beta^*)_s}{(\rho\beta^*)_f}\right), \\ x_4 &= \frac{3(\sigma - 1)\phi}{(\sigma + 1) - (\sigma - 1)\phi} + 1, x_5 = \phi \left[\frac{(\rho C_P)_s}{(\rho C_P)_f}\right] - \phi + 1, x_6 = \frac{k_s - 2\phi(k_f - k_s) + 2k_f}{k_s + \phi(k_f - k_s) + 2k_f}, \\ a_1 &= \frac{1}{(1 - \phi)^{2.5}x_1}, a_2 = \left[\frac{x_2}{x_1}\right], a_3 = \left[\frac{x_3}{x_1}\right], a_4 = \left[\frac{x_4}{x_1}\right], M^2 = \frac{\sigma_f B_0^2 v_f}{\rho_f u_0^2}, \\ Q_L &= \frac{Q_1 v_f^2 (C_w' - C_\infty')}{k_f u_0^2 (T_w' - T_\infty')}, Gr = \frac{g\beta_f v_f (T_w' - T_\infty')}{u_0^3}, So = \frac{D_1 (T_w' - T_\infty')}{v_f (C_w' - C_\infty')}, Kr = \frac{k_r^1 v_f}{u_0^2}, \\ Gc &= \frac{v_f g\beta_f^* (C_w' - C_\infty')}{u_0^3}, K^* = \frac{K u_0^2}{v_f^2}, Pr = \frac{\mu_f (C_P)_f}{k_f}, Nr = \frac{16\sigma_s T_\infty'^3}{3k_e k_f}, Sc = \frac{v_f}{D}. \end{split}$$

In non-dimensional quantities, the initial & boundary conditions are

$$U(Y,0) = 0, T(Y,0) = 0, C(Y,0) = 0 \quad \forall \quad Y$$

$$U(0,t) = \exp(at), T(0,t) = t, C(0,t) = t \quad \forall \quad t > 0$$

$$U(Y,t) \to 0, T(Y,t) \to 0, C(Y,t) \to 0 \quad \text{as} \quad Y \to \infty, t > 0$$
(14)

# 3. Numerical procedure

Equations (11)-(13) are  $2^{nd}$  order Linear coupled PDE together with both conditions from the equation (14). So equations (11)-(13) together with equation (14) are resolved by using the Crank-Nicolson implicit finite-difference scheme. Therefore, finite-difference equations are mentioned below:

$$-r_1U((m-1),(n+1)) + a_{11}U(m,(n+1)) - r_1U((m+1),(n+1))$$

$$= r_1U((m-1),n) + a_{12}U(m,n) + r_1U((m+1),n) + r_4T(m,n) + r_5C(m,n)$$
(15)

$$-r_{8}T((m-1),(n+1)) + b_{11}T(m,(n+1)) - r_{8}T((m+1),(n+1))$$

$$= r_{8}T((m-1),n) + b_{12}T(m,n) + r_{8}T((m+1),n) + r_{9}C(m,n)$$

$$-r_{10}C((m-1),(n+1)) + c_{11}C(m,(n+1)) - r_{10}C((m+1),(n+1))$$

$$= r_{10}C((m-1),n) + c_{12}C(m,n) + r_{10}C((m+1),n)$$

$$+ r_{11}T((m-1),n) - 2r_{11}T(m,n) + r_{11}T((m+1),n)$$
(17)

where

$$r_{1} = \frac{a_{1}\Delta t}{2(\Delta Y)^{2}}, r_{2} = M^{2}a_{4}\Delta t, r_{3} = \frac{a_{1}\Delta t}{K}, r_{4} = Gra_{2}\Delta t, r_{5} = Gca_{3}\Delta t, r_{6} = \frac{\Delta t}{x_{5}Pr},$$

$$r_{7} = \frac{x_{6} + Nr}{2(\Delta Y)^{2}}, r_{8} = r_{6}r_{7}, r_{9} = r_{6}Q_{L}, r_{10} = \frac{\Delta t}{2Sc(\Delta Y)^{2}}, r_{11} = \frac{So\Delta t}{(\Delta Y)^{2}}, r_{12} = Kr\Delta t$$

$$a_{11} = (1 + 2r_{1}), a_{12} = (1 - 2r_{1} - r_{2} - r_{3}), b_{11} = (1 + 2r_{8}), b_{12} = 1 - 2r_{8}, c_{11} = (1 + 2r_{10}),$$

$$c_{12} = (1 - 2r_{10} - r_{12}).$$

The difference equations are obtained by dividing the flow zone into a grid or mesh of lines horizontally and vertically along with the plate. The suffix m refers to Y and the suffix n to time. Taking  $\Delta Y = 0.1, \Delta t = 0.001, m_{\text{max}} = 200, n_{\text{max}} = 500$ , the mesh system is partitioned. The following is the equivalent of the first condition in equation (14).

$$U(m,0) = 0, T(m,0) = 0, C(m,0) = 0 \text{ for all } m$$
 (18)

The second condition from Equation (14) is expressed in finite-difference form as follows

$$U(0,n) = e^{a(n-1)\Delta t}, T(0,n) = (n-1)\Delta t, C(0,n) = (n-1)\Delta t \text{ for all } n$$

$$U(m_{\text{max}}, n) = 0, T(m_{\text{max}}, n) = 0, C(m_{\text{max}}, n) = 0 \text{ for all } n$$
(19)

Every internal node of each time step is a tridiagonal matrix when the equations (15)-(17) are combined with the abovementioned conditions from equations (18) and (19). The tridiagonal matrix has a dimension of  $(m_{max} - 1) \times (m_{max} - 1)$  (i.e.  $199 \times 199$ ). The Thomas method for solving  $(m_{max} - 1)$  equations with  $(m_{max} - 1)$  unknowns for each time step can be used to solve the tridiagonal matrix system of equations. We started by computing the concentration and temperature fields at each time step from equations (17) and (16), respectively, because it is a coupled equation, and then used the calculated values to compute the velocity field at each time step from equation (15), which meets the convergence criteria. The Nusselt number, Sherwood number, and friction factor are non-dimensional characteristics that may be determined using the formulae below.

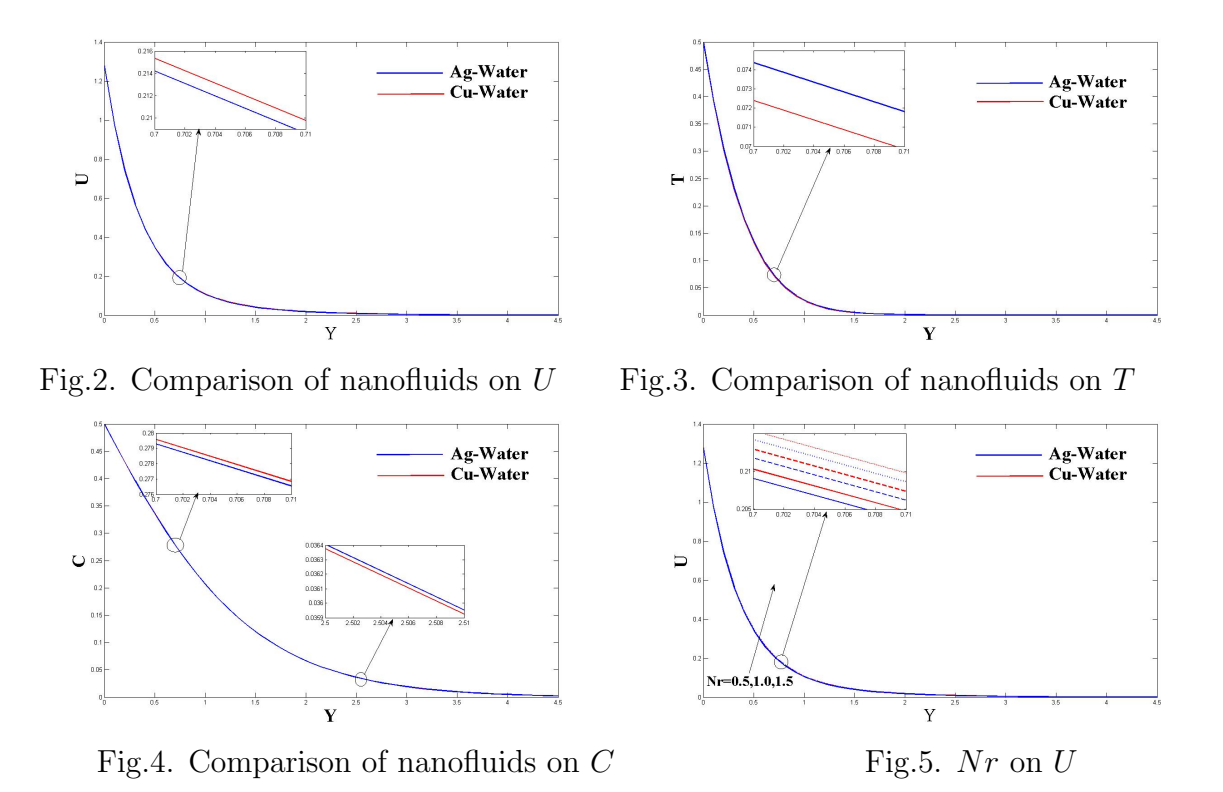
$$Nu = -\frac{\partial T}{\partial Y}, Sh = -\frac{\partial C}{\partial Y}, \tau = -\frac{\partial U}{\partial Y} \text{ at } Y = 0$$
 (20)

#### 4. Results and Discussion

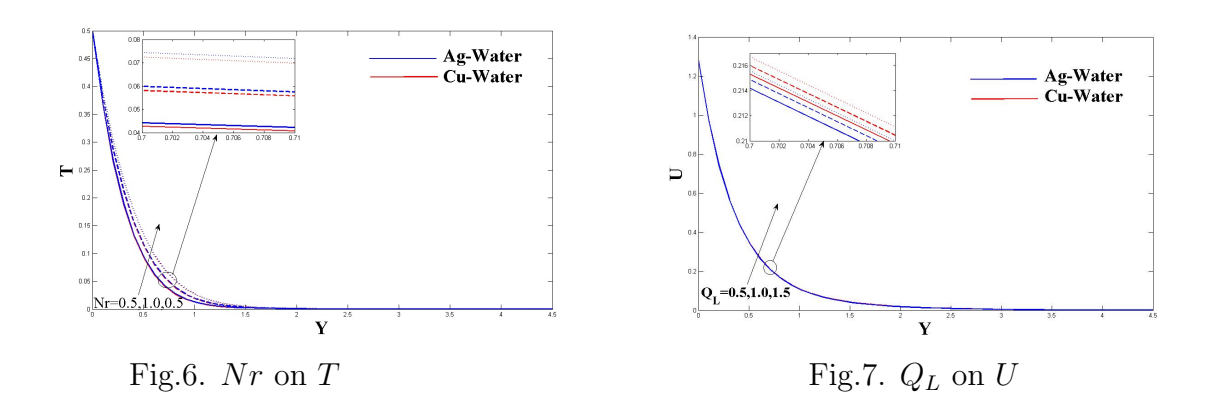
To gain a physical understanding of the problem, detailed numerical simulations for various values of the predominant factors such as solutal Grashof number (Gc), nanoparticle volume fraction  $(\phi)$ , thermal Grashof number (Gr), Prandtl number (Pr), radiation-absorption parameter  $(Q_L)$ , magnetic parameter (M), dimensionless time (t), radiation parameter (Nr), acceleration (a), permeability parameter  $(K^*)$ , Schmidt number (Sc), chemical reaction parameter (Kr), Soret number (So), Nusselt number (Nu), Sherwood number (Sh), and friction factor  $(\tau)$  are carried out and discussed through graphs and tables. Consider the following fixed values wherever they are needed during the computation.

$$Gr = 5, Gc = 5, \phi = 0.1, Pr = 6.8, Q_L = 0.5, M^2 = 10, Sc = 0.22, Nr = 1.5, K^* = 5, t = 0.5, a = 0.5, So = 1, Kr = 3.$$

The velocity distribution of both Silver (Ag) and Copper (Cu) water-based nanofluids with the same volume fraction parameter is shown in Fig. 2. Because of the considerably greater density of Ag from table 1, the Ag-water has a narrower boundary layer. This is owing to growth in its dynamic viscosity. Figs. 3-4 exhibit the temperature and species concentration distributions of both nanofluids. It is seen that thermal boundary layer thickness is higher in the case of Ag-water from fig. 3. But it is observed that the reverse pattern observed near the plate in the solutal boundary layer is shown in Fig. 4.

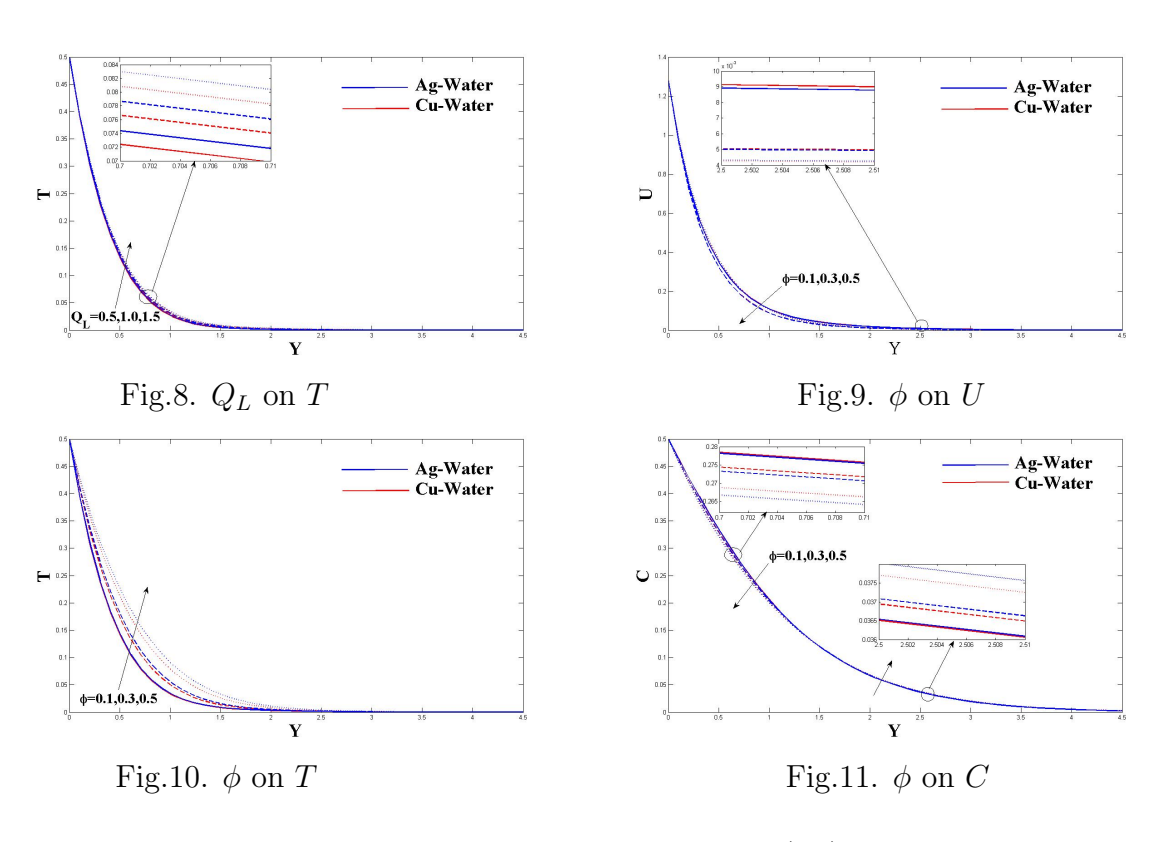


The impact of the radiation parameter (Nr) on the fluid velocity U and fluid temperature T reports of both nanofluids is seen in Figs. 5-6. U and T rise for various values of Nr. The thickening of the thermal boundary layer is responsible for the radiation factor. This allows the fluid to discharge heat energy from the flow zone, resulting in the chilling of the system. This is valid since the findings of the Rosseland approximation improve as the temperature rises.



Figs. 7-8 are sketched to show the behavior of radiation absorption  $(Q_L)$  on the fluid velocity and fluid temperature. Both fluid velocity and fluid temperature summary are rising for the augmented values of  $Q_L$ . The flow rate is increased due to the buoyant force caused when heat is absorbed. Therefore, the amount of radiation absorbed across the boundary layer thickness increases as the thickness of the momentum boundary layer increases.

Figs. 9-11 are presented the impact of volume fraction parameter ( $\phi$ ) on velocity, temperature, and species concentration of both nanofluids. Velocity and species concentration decelerate but the fluid temperature accelerates for the augmented values of the volume fraction parameter. Because when  $\phi$  rises, the thermal conductivity of the nanofluid increases, raising the fluid temperature. Because Agnanoparticles have high heat conductivity, they are ideal for this application. As a result, we infer that Cu-water nanofluid has a lesser fluid temperature than Agwater nanofluid.



Figs. 12-13 are describing the behavior of Soret number (So) on fluid velocity U and species concentration C reports. U and C are accelerated for the enlargement of the values of So. This is the result of a substantial mass diffusion effect caused

by a thermal gradient. Thermo diffusion is the movement of mass across a fluid as a result of a concentration gradient. This phenomenon might occur as a result of the presence of a thermal gradient. In general, the Soret effect is of a lower order of magnitude than Fick's law impact, therefore thus is frequently overlooked in mass transfer processes. Though the impact is minor, the devices may be set up to provide a very steep temperature gradient, which can affect the separation of components in mixes. Furthermore, we can see that the Cu-water based nanofluid has a larger concentration than the Ag-water based nanofluid. Figs. 14-15 are illustrating the influences of Kr on velocity U and species concentration C of the nanofluid. U and C are suppressed as increasing the values of Kr. Therefore, the values of Kr are increased, the rate of reaction between nanoparticles increases, and thus the nanoparticle concentration decay and the moment boundary layer decrease for both nanofluids.

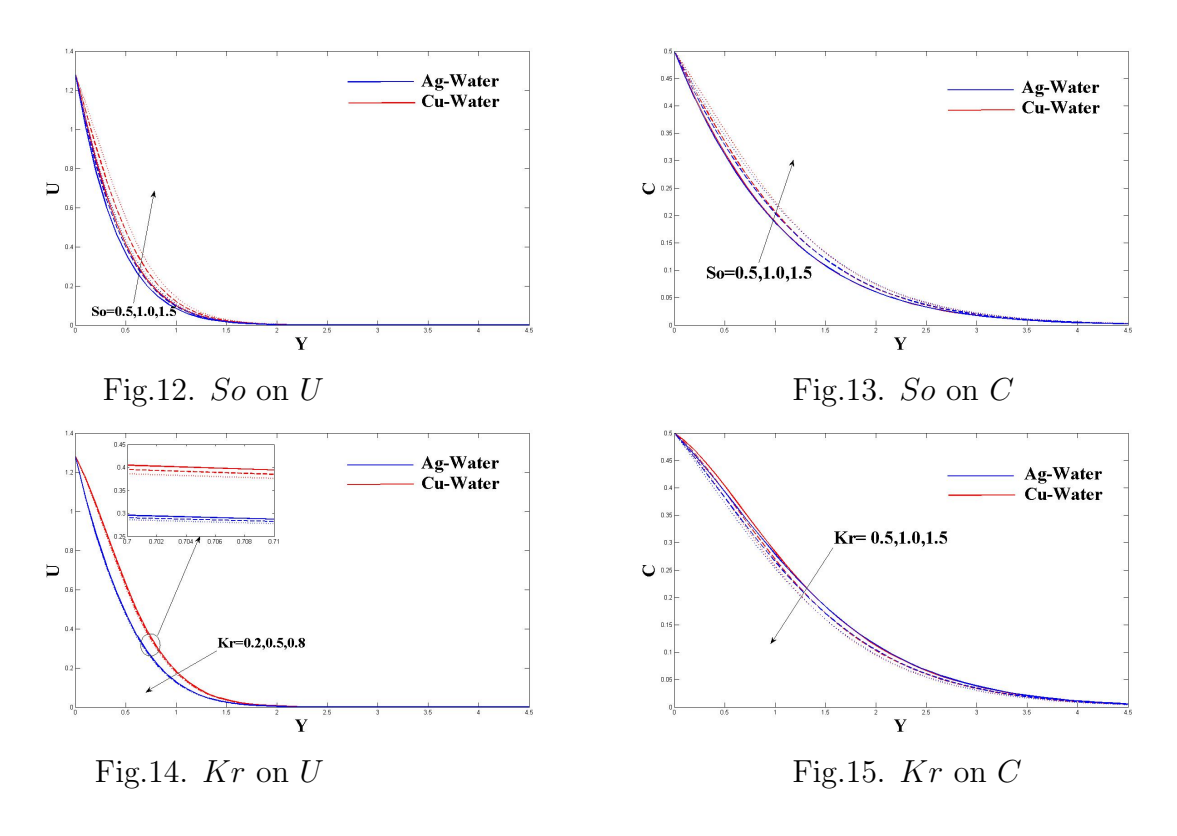


Table 2 exhibits the numerical values of the friction factor  $\tau$ , Nusselt number Nu and Sherwood number Sh for a variety of significant flow factors. It is seen that enlarging the values of Kr, the friction factor  $\tau$  at the wall upturns in both nanoparticles, but it decreases when the values of Nr,  $Q_L$ ,  $\phi$ , and So are increased.

For growing values of Nr,  $Q_L$ ,  $\phi$ , and So, Nusselt number Nu rises, whereas for enlargement values of Nr,  $Q_L$ ,  $\phi$ , and So, Nusselt number Nu decreases. In both nanofluids, Sherwood number Sh increases for enhancing Nr,  $Q_L$ ,  $\phi$ , and Kr, but decreases for So. The numerical results for different mess sizes are in good agreement with the finding of Rajesh et al. [10] from table 3.

Nr	$Q_L$	So	Kr	φ	τ		Nu		Sh	
					Cu	Ag	Cu	Ag	Cu	Ag
0.5	2	0.6	3	0.1	3.0416	3.0620	0.7704	0.7626	0.1908	0.1917
1.0					3.0376	3.0580	0.6990	0.6917	0.1994	0.2003
1.5			Į.	Į.	3.0344	3.0548	0.6451	0.6383	0.2059	0.2067
	0.5			Į.	3.0352	3.0556	0.6585	0.6517	0.2044	0.2052
	1.0			į.	3.0349	3.0553	0.6540	0.6472	0.2049	0.2057
	1.5				3.0346	3.0551	0.6496	0.6428	0.2054	0.2062
		0.5		Į	3.0356	3.0560	0.6497	0.6429	0.2152	0.2158
		1.0		Į	3.0308	3.0513	0.6490	0.6422	0.1663	0.1676
		1.5		Į.	3.0260	3.0465	0.6484	0.6415	0.1175	0.1195
			0.5	į.	3.0222	3.0429	0.6479	0.6411	0.0793	0.0814
			5	į.	3.0287	3.0492	0.6487	0.6419	0.1452	0.1472
			10		3.0346	3.0550	0.6495	0.6427	0.2059	0.2078
				0.1	3.0489	3.0690	0.6495	0.6427	0.2059	0.2078
			Į.	0.3	3.0269	3.0603	0.5658	0.5465	0.2292	0.2345
				0.5	2.6907	2.7144	0.4732	0.4441	0.2540	0.2616

Table 2. Friction factor, Nusselt number, and Sherwood number

Table 3. Comparison of friction factor (  $\tau$  ) for different values of  $\phi$ 

φ	Rajesh	et a1.[6]	Present study size dt=0. dY=0	001 and	Present study with step size dt=0.001 and dY=0.002		
		τ	τ				
	Cu	Ag	Cu	Ag	Cu	Ag	
0	-2.3523	-2.3523	-2.1971	-2.1971	-2.1833	-2.1833	
0.01	-2.4030	-2.4057	-2.2508	-2.2537	-2.2385	-2.2419	
0.02	-2.4551	-2.4607	-2.3057	-2.3116	-2.2947	-2.3015	
0.03	-2.5087	-2.5174	-2.3621	-2.3711	-2.3521	-2.3624	
0.04	-2.5639	-2.5757	-2.4198	-2.4322	-2.4108	-2.4246	

#### 5. Conclusion

The impact of the Soret and radiation-absorption parameters on magnetohy-drodynamic convective Ag and Cu water-based nanofluid flow via an accelerated exponentially vertical porous plate with changing temperature and concentration is investigated. The following are the study's most interesting findings:

1. The Nanofluid velocity increases for the augmented values of radiation parameter

Nr, radiation absorption parameter  $Q_L$ , and Soret number So, whereas decreases for enlargement of volume fraction parameter  $\phi$  and parameter of chemical reaction Kr.

- 2. Temperature of nanofluid gets elevation for radiation parameter Nr, radiation-absorption parameter  $Q_L$ , and volume fraction parameter  $\phi$ .
- 3. Species concentration of the nanofluid increases for So whereas decreases for volume fraction parameter  $\phi$  and chemical reaction parameter Kr.
- 4. Both Nusselt number and Shear stress coefficient (friction factor) increase for chemical reaction parameter Kr whereas decreases for radiation parameter Nr, radiation-absorption parameter  $Q_L$ , volume fraction parameter  $\phi$ , and Soret number So.
- 5. The Sherwood number is increased for radiation parameter Nr, radiationabsorption parameter  $Q_L$ , volume fraction parameter  $\phi$ , and chemical reaction parameter Kr whereas growing values of So reduce the Sherwood number.

### References

- [1] Ameer Ahamad, N., Veera Krishna, M. and Chamkha, A. J., Radiation-Absorption and Dufour Effects on Magnetohydrodynamic Rotating Flow of a Nanofluid Over a Semi-Infinite Vertical Moving Plate with a Constant Heat Source, Journal of Nanofluids, Vol. 9(3) (2020), 177-186.
- [2] Anwar, T., Kumam, P., Shah, Z., Watthayu, W. and Thounthong, P., Unsteady radiative natural convective MHD nanofluid flow past a porous moving vertical plate with heat source/sink, Molecules, Vol. 25(4) (2020), 854.
- [3] Choi, S. U. S. and Eastman, J. A, Enhancing Thermal Conductivity of Fluids with Nanoparticles, Argonne National Lab, Lemont, IL, USA, 1995.
- [4] Hamilton, R. L. and Crosser, O. K., Thermal conductivity of heterogeneous two-component systems, Industrial & Engineering chemistry fundamentals, Vol. 1(3) (1962), 187-191.
- [5] Krishna, M. V., Ahamad, N. A. and Chamkha, A. J., Radiation absorption on MHD convective flow of nanofluids through vertically travelling absorbent plate, Ain Shams Engineering Journal, (2021).
- [6] Mahanthesh, B., Gireesha, B. J. and Gorla, R. S. R., Heat and mass transfer effects on the mixed convective flow of chemically reacting nanofluid past a moving/stationary vertical plate, Alexandria Engineering Journal, 55(1) (2016), 569-581.

- [7] Mishra, A., Pandey, A. K., Chamkha, A. J. and Kumar, M., Roles of nanoparticles and heat generation/absorption on MHD flow of Ag-H<sub>2</sub>O nanofluid via porous stretching/shrinking convergent/divergent channel, Journal of the Egyptian Mathematical Society, Vol. 28(1) (2020), 283-294.
- [8] Prasad, P. D., Kumar, R. K., and Varma, S. V. K., Heat and mass transfer analysis for the MHD flow of nanofluid with radiation absorption, Ain Shams Engineering Journal, 9(4) (2018), 801-813.
- [9] Rajesh, V., Mallesh, M. P. and Sridevi, C., Transient MHD nanofluid flow and heat transfer due to a moving vertical plate with thermal radiation and temperature oscillation effects, Procedia Engineering, Vol. 127 (2015), 901-908.
- [10] Rajesh, V., Debnath, L. and Chakrala, S., Unsteady MHD free convection flow of nanofluid past an accelerated vertical plate with variable temperature and thermal radiation, International Journal of Applied and Computational Mathematics, Vol. 3(2) (2017), 1271-1287.
- [11] Raju, A. M., Reddy, P. C., Mallikarjuna, B. and Raju, C. S. K., Radiation Absorption and Soret Effects on MHD Conduction Fluid Flow Past an Exponentially Accelerated Vertical Plate, South East Asian J. of Mathematics and Mathematical Sciences, Vol. 16(3) (2020), 67-74.
- [12] Reddy, P. C., Raju, M. C., Raju, G. S. S. and Varma, S. V. K., Free convective magneto-nanofluid flow past a moving vertical plate in the presence of radiation and thermal diffusion, Frontiers in Heat and Mass Transfer, Int. Journal, Vol. 7(1) (2016), 28.
- [13] Reddy, P. C., Raju, M. C. and Raju, G. S. S., Free Convective Heat and Mass Transfer Flow of Heat-Generating Nanofluid Past a Vertical Moving Porous Plate in a Conducting Field, Special Topics & Reviews in Porous Media: An International Journal, 7(2) (2016).
- [14] Reddy, P. C., Venkateswara Raju, K., Umamaheswar, M. and Raju, M. C., Buoyancy Effects on Chemically Reactive Magnetonanofluid Past a Moving Vertical Plate, Bull. Pure Appl. Sci. Math. Stat, Vol. 38e (2019), 193-207.
- [15] Sailaja, B., Srinivas, G., Suresh Babu, B. and Kiran Kumar, G., Free and Forced Convective Heat Transfer Through a Nanofluid in Two dimensions

- Past Moving Vertical Plate, South East Asian J. of Mathematics and Mathematical Sciences, Vol. 16(1A) (2020), 67-74.
- [16] Satya Narayana, P. V., Venkateswarlu, B. and S. Venkataramana, S., Thermal Radiation and Heat Source Effects on a MHD Nanofluid Past a Vertical Plate in a Rotating System with Porous Medium, Heat Transf. - Asian Res., Vol 44(1) (2015), 1-19.
- [17] Satya Narayana, P. V., Venkateswarlu, B., Heat and mass transfer on MHD nanofluid flow past a vertical porous plate in a rotating system, Frontiers in Heat and Mass Transfer (FHMT), Vol 7(1) (2016).
- [18] Satya Narayana, P. V., Effects of variable permeability and radiation absorption on magnetohydrodynamic (MHD) mixed convective flow in a vertical wavy channel with traveling thermal waves, Propulsion and Power Research, Vol. 4(3) (2015), 150-160.
- [19] Sheikholeslami, M., Kataria, H. R. and Mittal, A. S., Effect of thermal diffusion and heat-generation on MHD nanofluid flow past an oscillating vertical plate through porous medium. Journal of Molecular Liquids, Vol. 257 (2018), 12-25.
- [20] Singha, A. K., Seth, G. S., Bhattacharyya, K., Yadav, D., Verma, A. K., and Gautam, A. K., Soret and Dufour effects on hydromagnetic flow of  $H_2O$ -based nanofluids induced by an exponentially expanding sheet saturated in a non-Darcian porous medium, Journal of Nanofluids, 10(4), (2021), 506-517.
- [21] Singh, J. K., Kolasani, S., and Seth, G. S., Heat and mass transport nature of MHD nanofluid flow over a magnetized and convectively heated surface including Hall current, magneto and thermo diffusions impacts, Ricerche di Matematica, 1-21 (2022).
- [22] Venkateswarlu, S., Varma, S. V. K. and Durga Prasad, P., MHD Flow of  $MoS_2$  and MgO water-based nanofluid through porous medium over a stretching surface with Cattaneo-Christov heat flux model and convective boundary condition, International Journal of Ambient Energy, (2020), 1-10.
- [23] Venkateswarlu, B. and Narayana, P. S., Chemical reaction and radiation absorption effects on the flow and heat transfer of a nanofluid in a rotating system, Applied Nanoscience, Vol. 5(3) (2015), 351-360.